Journal of Computer-Aided Molecular Design, **16:** 213–225, 2002.
KLUWER/ESCOM

Computational study of the catalytic domain of human neutrophil collagenase. Specific role of the S_3 and S'_3 subsites in the interaction with a phosphonate inhibitor

Massimiliano Aschi[a], Danilo Roccatano[a], Alfredo Di Nola[b], Carlo Gallina[c], Enrico Gavuzzo[d], Giorgio Pochetti[d], Michael Pieper[e], Harald Tschesche[e] & Fernando Mazza[a,d,*]
[a]*Dipartimento di Chimica, Ingegneria Chimica e Materiali, Università degli Studi, V. Vetoio, 67010 L'Aquila, Italy;* [b]*Dipartimento di Chimica, Università degli Studi 'La Sapienza', P. A. Moro 5, 00185 Roma, Italy;* [c]*Dipartimento di Scienze del Farmaco, Universita G. d'Annunzio, V. dei Vestini, 66100 Chieti, Italy;* [d]*Istituto di Strutturistica Chimica, CNR, C.P. n. 10, 00016 Monterotondo Stazione, Roma, Italy;* [e]*Fakultät für Chemie, Abteilung Biochemie I, Universität Bielefeld, Universitätstrasse 25, D-33615 Bielefeld, Germany*

Received 30 January 2002; Accepted 29 May 2002

Key words: enzyme-inhibitor binding, essential dynamics, human neutrophil collagenase, molecular dynamics

Summary

Human neutrophil collagenase (HNC, MMP-8) is one of the target enzymes for drug treatment of pathologic extracellular matrix degradation. Peptidomimetic inhibitors bind in the S′-side of the enzyme active site occupying the S'_1 primary specificity pocket by their large hydrophobic side-chains. The crystal structure of the complex between the catalytic domain of MMP-8 and Pro-Leu-L-$Trp^P(OH)_2$ (PLTP) showed that this phosphonate inhibitor binds in the S side of the active site. This finding was unexpected since it represents the first example of accommodation of the bulky Trp indolyl chain in the S_1 rather than in the S'_1 subsite. Dynamical and structural factors favouring this uncommon mode of binding were therefore investigated.

MD simulations performed on the uncomplexed enzyme show that its structure in aqueous solution is only slightly different from the crystal structure found in the complex with PLTP. ED analysis of the MD simulations, performed on PLTP alternatively interacting with the S- or S′-side of the active site, shows that the enzyme fluctuation increases in both cases. The main contribution to the overall enzyme fluctuation is given by the loop 164–173. The fluctuation of this loop is spread over more degrees of freedom when PLTP interacts with the S-side. This dynamical factor can enhance the preference of PLTP for the S subsites of MMP-8. MD simulations also show that ligation of PLTP in the S subsites is further favoured by better zinc chelation, a cation-π interaction at the S_3 subsite and unstrained binding conformations. The role of the S_3, S'_3 and S'_1 subsites in determining the inhibitor binding is discussed.

Abbreviations: ED – essential dynamics; FLTP – *N*-[(furan-2-yl)carbonyl]-Leu-L-$Trp^P(OH)_2$; MD – molecular dynamics; MMP-2 – gelatinase A; MMP-3 – stromelysin; MMP-8 – human neutrophil collagenase; MMP-9 – gelatinase B; PLTP – Pro-Leu-L-$Trp^P(OH)_2$.

Introduction

Reprolysins and matrix metalloproteinases (MMPs) present very similar zinc-dependent catalytic domains and high degree of conservation of the tertiary structure at the active site [1–4]. Thus, some Trp containing tripeptides, found in snake venoms, behave as weak and competitive inhibitors for both reprolysins and MMPs [5]. This finding suggested that we could modify the structure of these endogenous peptides,

*To whom correspondence should be addressed. E-mail: mazza@univaq.it

rather than that of natural substrates, with the aim of increasing potency and selectivity against MMPs.

The *N*-[(furan-2-yl)carbonyl]-Leu-L-Trp^{P}(OH)$_2$ phosphonate inhibitor (FLTP) was about 100-fold more potent than the carboxylate analog against adamalysin [6, 7], considered as the reprolysin prototype [8, 9]. The crystal structure of adamalysin complexed with FLTP [10] showed that the phosphonate group binds the catalytic zinc ion and the peptide backbone occupies the S′-side of the active site, inserting the Trp side-chain into the deep primary specificity pocket S_1'.

Further chemical modifications, replacing the furan ring of FLTP by pentatomic heterocyclic aromatic and non-aromatic rings, led to new phosphonate analogues tested as inhibitors of adamalysin, MMP-2, MMP-3, MMP-8 and MMP-9 [11]. Among the other analogues, PLTP showed an interesting increase of affinity against MMP-8, while its potency against adamalysin decreased. The crystal complex MMP-8:PLTP [12] revealed that while the zinc chelation by the phosphonate group is very similar to that found in the adamalysin:FLTP complex, unexpectedly the inhibitor peptide backbone occupies the S-side of the active site, leaving the primary specificity S_1' pocket unfilled. The occupation of the S region could not be attributed to the shrinkage of the bottleneck entrance of S_1' pocket of MMP-8. This is 0.80 nm [12] while that of adamalysin is 0.86 nm [10]. The small shrinking of 0.06 nm should not prevent the insertion of the indole ring into the S_1' pocket of MMP-8. In fact, HNC can still hydrolyze substrates containing Trp at P_1' [13–15]. Moreover, widening of this entrance up to 0.90 nm was evidenced in the crystal of MMP-8 complexed with a sulfonamide inhibitor [12].

In order to explain the unexpected preference of PLTP for the S subsites of MMP-8, we have investigated the dynamical and structural factors affecting its binding to both sides of the active site. To this purpose we first analyzed the structure of the uncomplexed MMP-8 in aqueous solution by MD simulation. Then two different simulations of PLTP interacting with the MMP-8 S- and S′-side, respectively were carried out. Finally, in order to ascertain the effect of enzyme-ligand interaction on PLTP fluctuation, the dynamics of free PLTP in aqueous solution was compared with those of the inhibitor interacting with the two sides of the active site.

Computational methods

Atomic coordinates

Since crystallographic data of uncomplexed MMP-8 were not available, we choosed the structure found in the crystal complex MMP-8:PLTP [12] (PDB code 1I73) as starting model for MD simulation. The free enzyme was obtained replacing the phosphonate inhibitor by a water molecule coordinated to the catalytic zinc ion. The MD simulation of PLTP interacting with the S-side of the active site started from the crystal structure of the MMP-8:PLTP complex. The initial position of the inhibitor interacting with the S′-side was modeled on the base of the crystal complex adamalysin:FLTP [10, 16–17]. A superimposition between the crystal structures of adamalysin and MMP-8 were done considering only the invariant parts of their active sites, namely the catalytic zinc ion and the three imidazole rings of the His residues coordinating the metal. The coordinates of PLTP were resumed from those of FLTP replacing the furan by a proline ring. This initial model was potential energy minimized by GROMOS87 force field [18] to prevent short contacts with the protein.

Force field parameters

The GROMOS87 force field [18] was used with increased repulsion between water oxygen and carbon atoms. Methyl, methylene and methyne hydrogens were treated as united atoms [18] together with each bound carbon, whereas the polar and aromatic hydrogens were explicitly treated to correctly account for the electrostatic interactions. The parameters of Merz and coworkers [19] with unitary partial charge were adopted for the zinc atom. The charges of the inhibitor were obtained by a standard Mulliken population analysis carried out on the corresponding HF/6-31G wavefunction optimized on the structure extracted from the crystal complex MMP-8:PLTP [12]. The charges obtained using electrostatic potential fitting the electronic density (CHELPG protocol) [20] and reported in Table 1, did not show significant differences from those obtained using the traditional Mulliken analysis. The calculations were carried out using the Gamess USA program [21].

Table 1. Partial atomic charges of the PLTP atoms used for the MD simulations. The atomic numbering scheme is reported in Figure 2.

No.	Atom Type	Residue	Charge (q/e)
0	H	PRO	0.30
1	H	PRO	0.30
2	N	PRO	−0.20
3	CH	PRO	0.20
4	CH_2	PRO	0.10
5	CH_2	PRO	0.10
6	CH_2	PRO	0.20
7	C	PRO	0.38
8	O	PRO	−0.38
9	N	LEU	−0.28
10	H	LEU	0.28
11	CH	LEU	0.00
12	CH_2	LEU	0.00
13	CH	LEU	0.00
14	CH_3	LEU	0.00
15	CH_3	LEU	0.00
16	C	LEU	0.38
17	O	LEU	−0.38
18	N	TRP	−0.28
19	H	TRP	0.28
20	CH	TRP	0.00
21	CH_2	TRP	0.00
22	C	TRP	−0.14
23	C	TRP	−0.14
24	H	TRP	0.14
25	C	TRP	0.00
26	N	TRP	−0.05
27	H	TRP	0.19
28	C	TRP	0.00
29	C	TRP	−0.14
30	H	TRP	0.14
31	C	TRP	−0.14
32	H	TRP	0.14
33	C	TRP	−0.14
34	H	TRP	0.14
35	C	TRP	−0.14
36	H	TRP	0.14
37	P	PO_3	1.00
38	0	PO_3	−1.00
39	0	PO_3	−1.00
40	0	PO_3	−1.00

Simulation protocol

The enzyme was initially put into a cubic box of 5 nm length at a distance larger than 0.7 nm from the walls. The box was filled by water molecules, described by the single point charge model [22] and Na^+ counterions to ensure electroneutrality of the system. Water molecules were initially energy minimized using a steepest descent procedure followed by 20 ps of MD run with geometrical constraints applied to the enzyme and, whenever present, also to the inhibitor. The overall system was then slowly heated from 50 K to 300 K and simulations of 1600 ps were finally carried out. The temperature was kept constant by the isogaussian algorithm [23]. Periodic boundary conditions were systematically applied and a cut-off of 1.2 nm was considered when coulombic and Lennard–Jones (LJ) forces were computed. The algorithm SHAKE [24] was used to constrain bond lengths allowing a longer integration step of 2 fs and the roto-translation constraint [25] was also adopted for the simulations.

ED [26] analysis of the trajectories of the C^α atom cartesian coordinates was carried out to study the enzyme fluctuation. This method allows the characterization of a configurational space, the essential space, in which the principal motions of the enzyme occur. The analysis consists in building the covariance matrix of the atomic positional fluctuations obtained from MD simulations. After its diagonalization, an orthonormal set of vectors (eigenvectors) is generated defining a new set of generalized coordinates. The essential subspace is defined by the eigenvectors with the largest eigenvalues of the atomic positional fluctuations covariance matrix [26].

O···H distances shorter than 0.25 nm and O-H···O angles larger than 60° were the criteria adopted for acceptance of hydrogen bonds. H-bond occurrence was reported as percentage of simulation time with respect to the last 800 ps of the trajectories after equilibrated simulation. The interaction involving a cationic species and the center of the mass of an aromatic partner, at a distance shorter than 0.6 nm, irrespective of the relative orientation, was considered as a cation-π interaction. This kind of interaction is not explicitly included in classical force fields.

A simulation of free PLTP in aqueous solution was also carried out adopting the same protocol. The fluctuation analysis was performed for 800 ps after equilibrated simulation.

All the simulations and analyses of the trajectories were performed using the GROMACS package [27].

Results and discussion

Modelling the catalytic zinc ion-water oxygen bond

Two different simulations, each of 1600 ps, were performed on the uncomplexed enzyme. In the first, the zinc-water oxygen bond was described in terms of coulombic and LJ interactions only, whereas in the other one, we considered an explicit covalent bond of 0.2 nm [19]. No significant difference was observed in the two cases; the water molecule, even if not covalently bound to the zinc ion, always maintained the same distance, of about 0.20 nm. This could be ascribed to the net atomic charges attributed to both zinc ion and water oxygen causing a strong coulombic interaction. Therefore the following analyses were carried out considering the catalytic zinc ion covalently bound to the water oxygen.

Uncomplexed enzyme structure in aqueous solution

A ribbon-type plot of MMP-8, deduced from the MMP-8:PLTP crystal complex, is shown in Figure 1 together with the sequence numbering of some residues involved in the discussion. The active site cleft of the catalytic domain separates the larger N - terminal subdomain from the smaller C-terminal one. The N-terminal subdomain is composed of a twisted five-stranded β-pleated sheet, bridged loops and two α-helices. The β-pleated sheet presents four parallel and one antiparallel strands; the only anti parallel strand, the 'edge' strand Leu 160-Phe 164, forms the upper (according to the view of Figure 1) rim of the active-site cleft. The S-shaped loop Gln 144-Leu 160, before entering the antiparallel strand, forms the 'bulge' segment Gly 155-Leu 160 protruding into the active site cleft. Both 'edge' strand and 'bulge' segment are regions important for substrate and inhibitor binding. The active-site helix, positioned below the 'edge' strand, contains His 197 and His 201 and extends to Gly 204 where the backbone turns from the helix towards His 207. The catalytic zinc ion, at bottom of the active-site, is coordinated by the $N^{\varepsilon 2}$ atoms of the three His residues 197, 201 and 207 belonging to the zinc binding consensus sequence 197–207 common to the 'metzincins' [2–4]. The C-terminal subdomain is organized less regularly in two wide loops and an α-helix.

A perspective view of the inhibitor PLTP conformation, found in the crystal complex MMP-8:PLTP, is reported in Figure 2; the adopted numbering scheme of the ligand and labelling of interacting protein residues are also reported. In the MD simulation, the root mean square deviation (rmsd) was computed by superimposing the C^{α} atoms of the structure simulated in aqueous solution with those of the crystal structure adopted as reference. As shown in Figure 3, the rmsd increases during the simulation and, after about 1100 ps, it reaches a plateau at 0.22 nm. The secondary structure elements, analyzed by the DSSP [28] method, were preserved during the simulation. The radius of gyration of native MMP-8 was fairly constant throughout the simulation, showing oscillations not exceeding 0.01 nm around the average of 1.45 nm.

The root mean square fluctuation (rmsf) of the backbone C^{α} atoms of MMP-8 is reported as blue line in Figure 4. It is interesting to observe that α-helices and β-strands indicated by vertical lines above and below the zero, respectively are fairly rigid. In particular, both active site essential elements, the α-helix containing His 197 and His 201 and the 'edge' strand, show the lowest fluctuations even in the absence of inhibitor. The unstructured parts of the enzyme that are completely exposed to the bulk solvent show pronounced fluctuation reaching the maximum in correspondence of the loops 144–160 and 164–173. It is interesting to observe that although these highly fluctuating loops include the 'edge' strand forming the upper rim of the active site, the rigidity of this β-strand is conferred by the H-bonding network of the five-stranded β-sheet. At variance with other enzymes, like for example citrate synthase [29], the inhibitor does not induce significant conformational changes upon binding to the active-site. The close resemblance between the crystal structure of MMP-8 and that simulated in aqueous solution, even in the absence of the inhibitor, renders the X-ray structure of this enzyme, and possibly other MMPs, particularly suitable for molecular modelling studies of new inhibitors.

Modelling the catalytic zinc ion-phosphonate oxygen bond

While the zinc-water oxygen interaction has been described as a covalent bonding in the MD simulation of the uncomplexed enzyme, for the zinc-phosphonate oxygen interaction we included the coulombic and LJ terms only. The inclusion of an explicit covalent term would indeed strongly affect MD simulations, hampering calculations of the subtle differences expected for PLTP interacting with S- and S′-side of the active site. It should be remarked that the initial zinc-phosphonate oxygen distance of 0.20 nm increases up

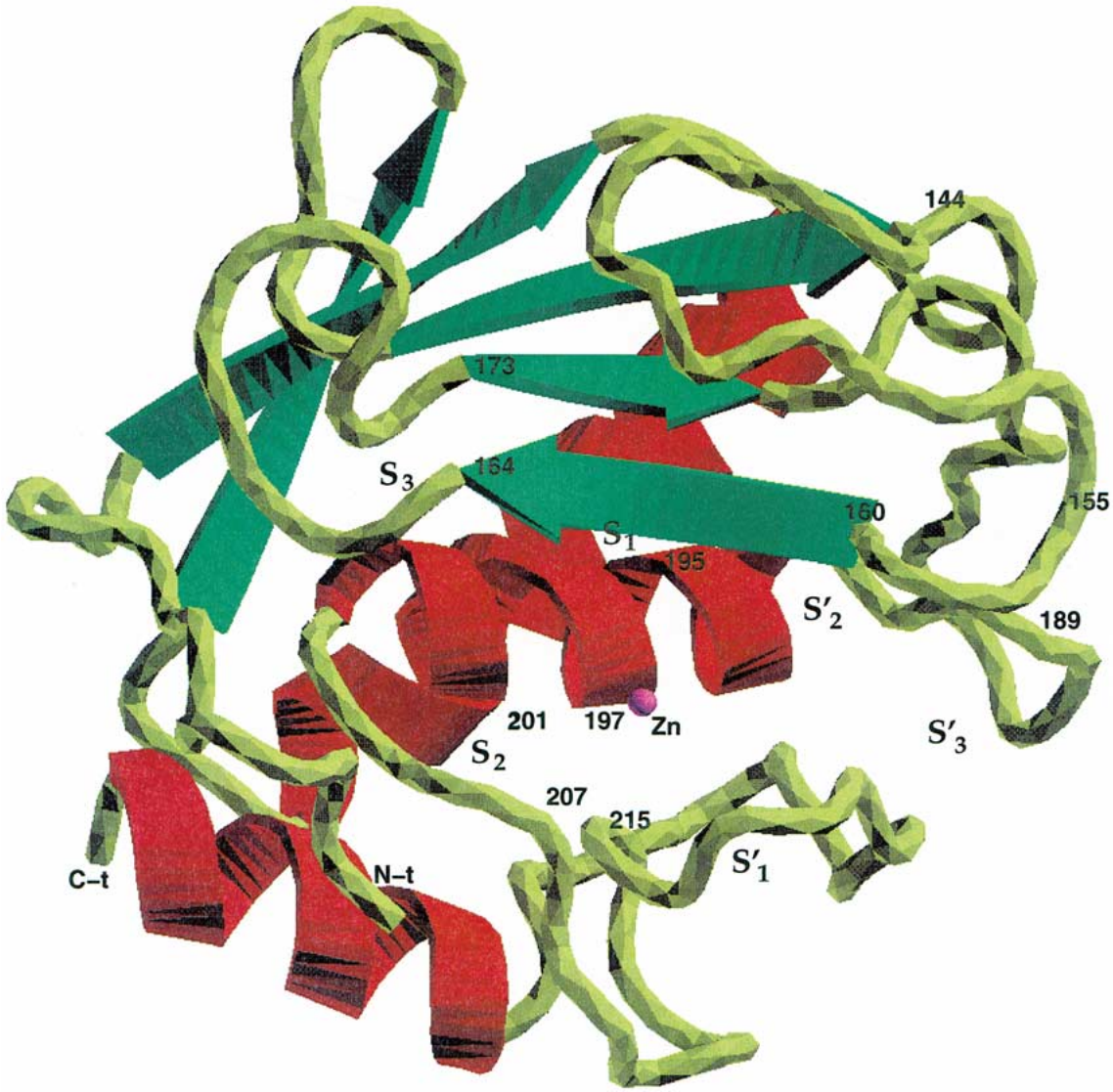

Figure 1. Ribbon-type plot of MMP-8. Helices are represented as helical ribbons, β-strands as twisted arrows and unstructured parts as ropes. The catalytic zinc ion and the numbering of some residues useful for discussion are indicated.

to 0.38 nm, after preliminary potential energy minimization. This could be ascribed to limitations of the classical description of the coordination bond, being underestimated with respect to simultaneous interactions of other groups of the inhibitor with the active site.

Effect of the inhibitor on enzyme fluctuation

The simulated interaction of PLTP with the S- and S′-side of the active site modifies the enzyme fluctuation. This effect can be appreciated by comparing the rmsf of C^{α} atoms of the uncomplexed enzyme, shown as blue line in Figure 4, with those of the two S- and S′-side PLTP-enzyme bound states reported as green and red lines, respectively in the same Figure. While a similar behaviour characterizes the sequences 80–144 and 180–242 of the three systems, the loops 144–160 and 164–173 of both bound states, are affected by a significant decrease and increase of fluctuation, respectively. It is worth to observe that the ligand interaction with either side of the active site causes a similar effect on the enzyme fluctuation.

ED analysis can give a deeper insight on the enzyme fluctuation. Figure 5 reports the fluctuations,

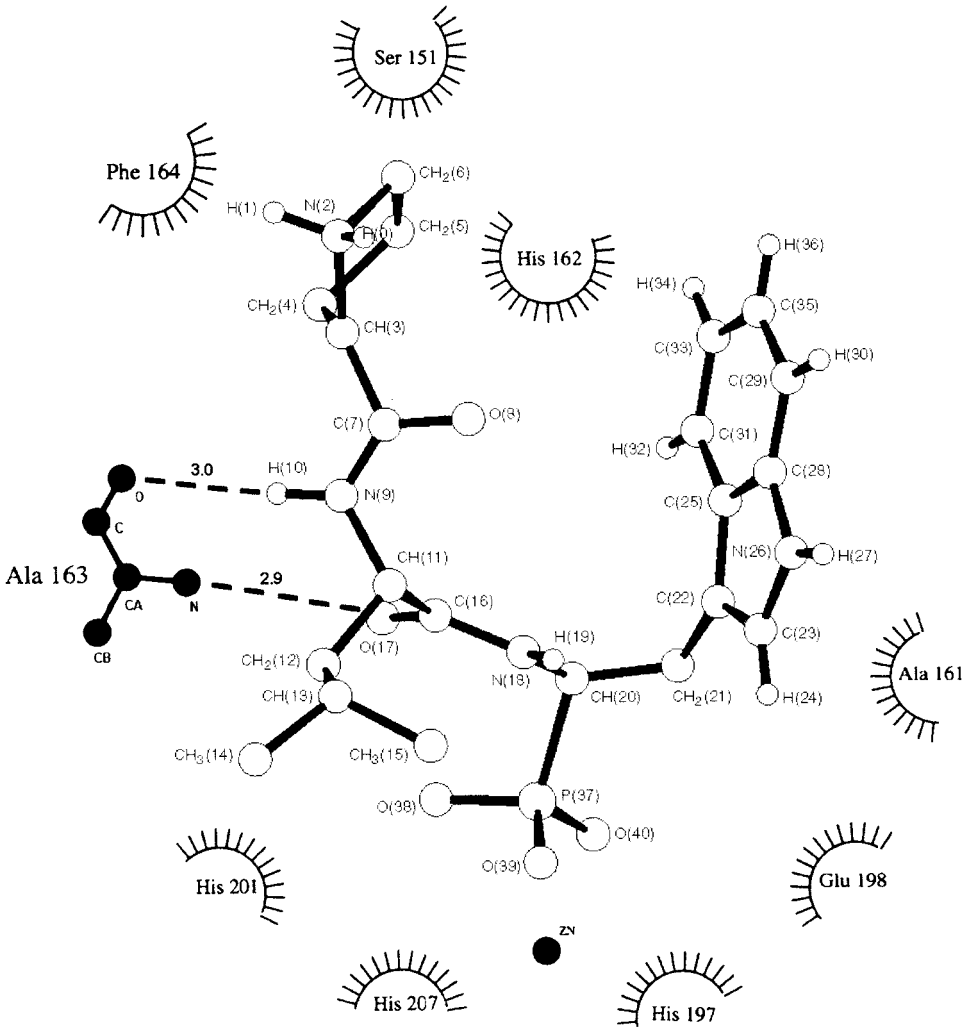

Figure 2. Perspective view of the inhibitor PLTP conformation found in the crystal complex MMP-8:PLTP. The atomic numbering scheme and labelling of the intervening protein residues are indicated. The omitted H atoms have been treated as united atoms together with each bound C atom in the MD simulation.

relative to the overall motion of the system, along the single eigenvectors for the three simulations. The curves were obtained from the values of the corresponding eigenvalues shown in the inset of Figure 5. The sums of the eigenvalues, related to the overall fluctuations, are 0.63 nm^2 for the uncomplexed enzyme, 0.92 and 0.88 nm^2 for S- and S′-side PLTP-enzyme bound states, respectively. The overall fluctuations of both bound states are similar and larger than that of the uncomplexed enzyme. Moreover, as can be seen from the plot, while 70% of the overall fluctuation of the uncomplexed enzyme is included in the first twenty eigenvectors, both PLTP-enzyme bound states distribute the same amount of overall fluctuations in a configurational space half smaller. The bound ligand confines the enzyme larger fluctuations in a smaller essential space.

Figure 6 reports the components of the first five eigenvectors of the trajectories obtained for the uncomplexed enzyme (blue line), S- (green line) and S′-side (red line) PLTP-enzyme bound states. For each C^{α} atom the value $\sqrt{(x_i^2 + y_i^2 + z_i^2)}$ is given, where (x_i, y_i, z_i) are the cartesian components of *i*th atom in the respective eigenvectors. When PLTP interacts with the S′-side (red line of Figure 6), the motion of loop 164–173 is mainly described by the first two eigenvectors, whereas the same fluctuation is described also by the third eigenvector (green line of Figure 6) when

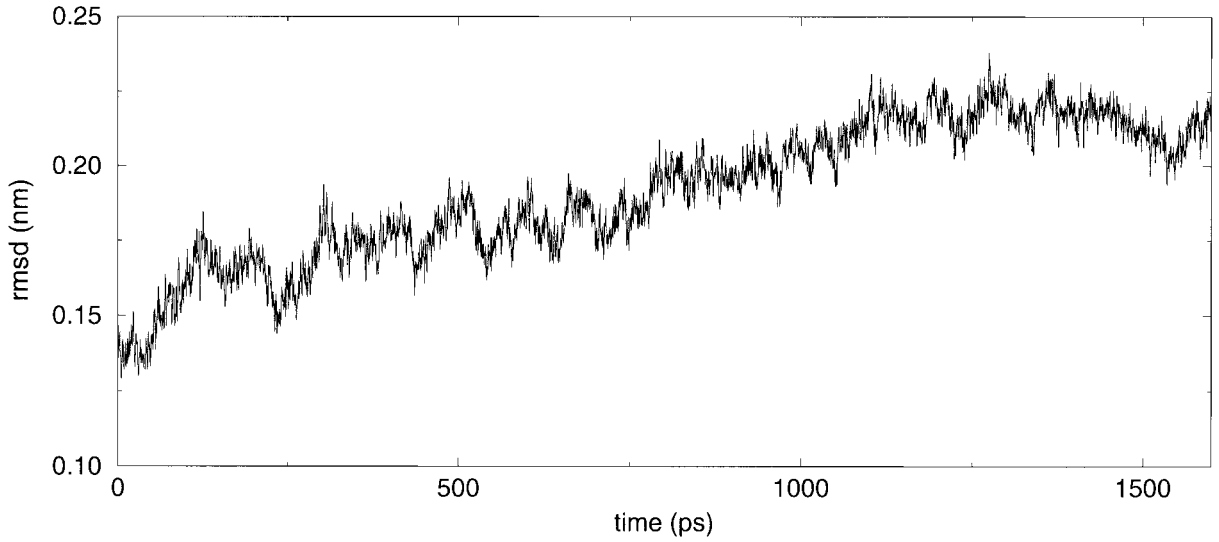

Figure 3. Time course of the root-mean square deviation (rmsd) of uncomplexed MMP-8. The curve has been obtained by superimposing the C^{α} atoms of the structure simulated in aqueous solution with those of the MMP-8:PLTP crystal complex.

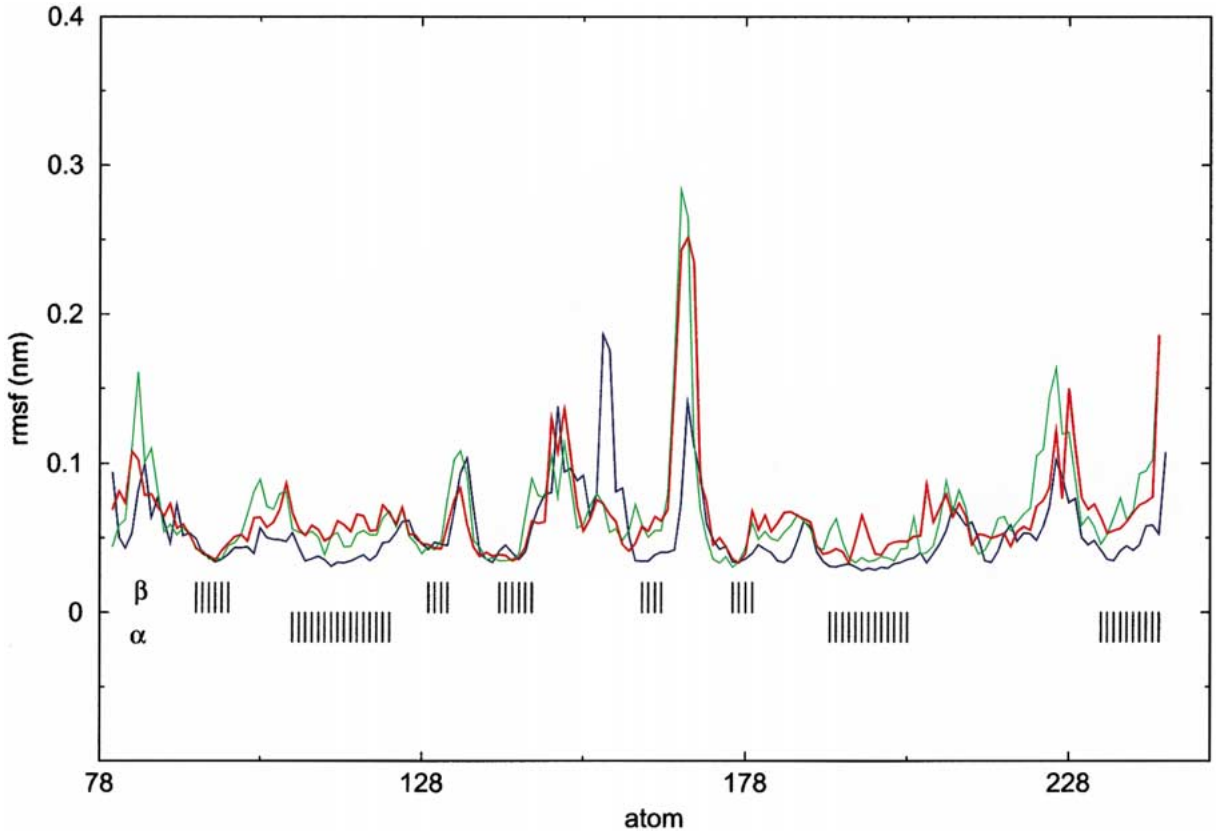

Figure 4. Root-mean square fluctuation (rmsf) of the C^{α} atoms of uncomplexed MMP-8 (blue line), S-side (green line) and S′-side (red line) PLTP-enzyme bound states. The secondary structure elements are indicated by vertical lines above and below the zero for α-helixes and β-strands, respectively.

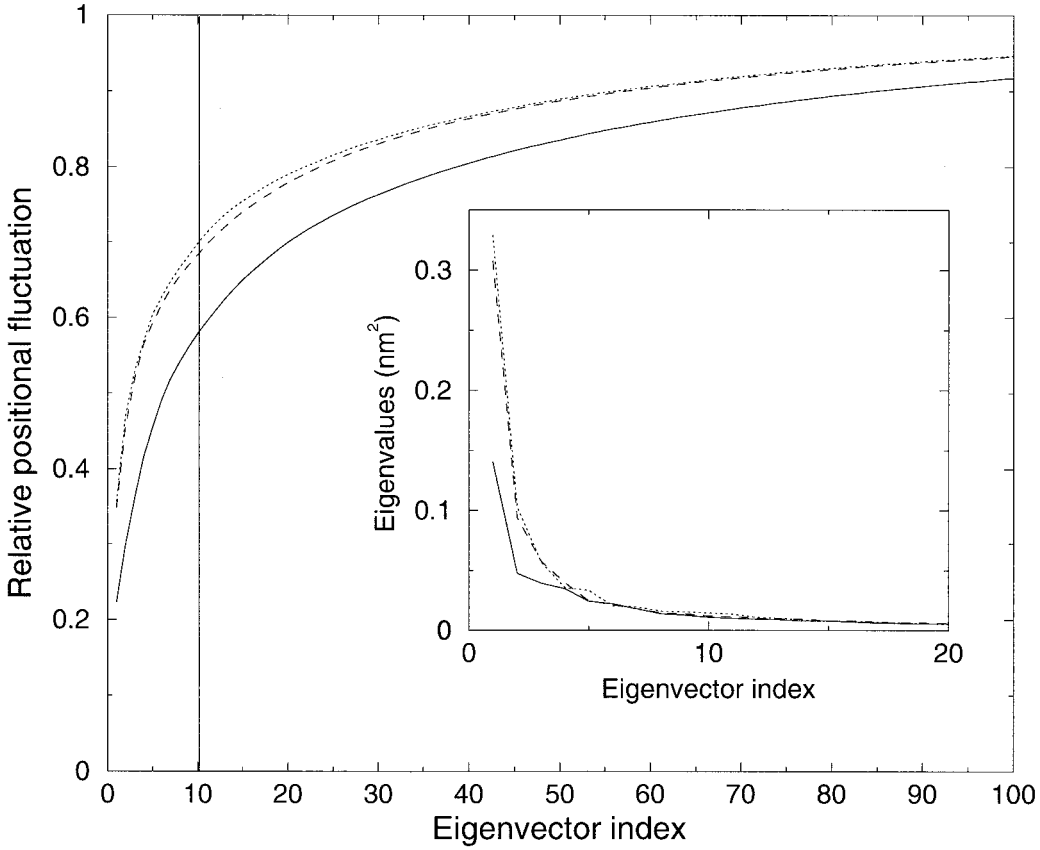

Figure 5. Plot of the relative positional fluctuation of the eigenvectors. The eigenvalues obtained from the C^{α} coordinates matrix of different simulations are reported, in decreasing order of magnitude, in the inset. Solid line refers to uncomplexed MMP-8, dashed and dotted lines refer to S- and S′-side PLTP-enzyme bound states, respectively.

the S-side is involved by the ligand. It is interesting to observe that the larger number of eigenvectors, describing the same type of motion, can contribute to render the PLTP interaction with the S-side more probable.

Crystallographic B factors measure the atomic motions and can be compared with the atomic fluctuations. The B parameter is related to the mean square fluctuation by $B = 8/3\pi^2 \langle \Delta r^2 \rangle$. The B factors of the enzyme C^{α} atoms, obtained from isotropic refinement of the X-ray data collected at 100 K on the crystal complex MMP-8:PLTP [12], are compared with those simulated at 300 K and reported in Figure 7. As expected, the amplitude of atomic motion significantly increases at room temperature, however a similar trend is maintained in the two cases. Apart from the N and C terminal parts, only few residues of the central loop 164–173 show very large fluctuation; the very small B values obtained from diffraction data for these residues can reflect crystal packing conditions not present in the structure simulated in aqueous solution.

Enzyme-ligand interactions at the S side

In the MD simulation of PLTP interacting with the S region, the distance between the catalytic zinc ion and the inhibitor phosphonate oxygen as well as that between the center of Phe 164 aromatic ring and the inhibitor Pro N were monitored. Averages of 0.38 nm and 0.50 nm, with 10% fluctuation around their values, were obtained in the two cases, respectively. Maintenance of Zn-O coordination with a value (0.38 nm) larger than that observed can be ascribed to underestimation of this interaction, as above discussed. The distance of 0.50 nm, between the protonated N of inhibitor Pro ring and the center of Phe 164 π-cloud, is indicative of a cation-π interaction stabilizing the complex formation at this region. Moreover, the inhibitor Leu NH and CO groups are engaged in two

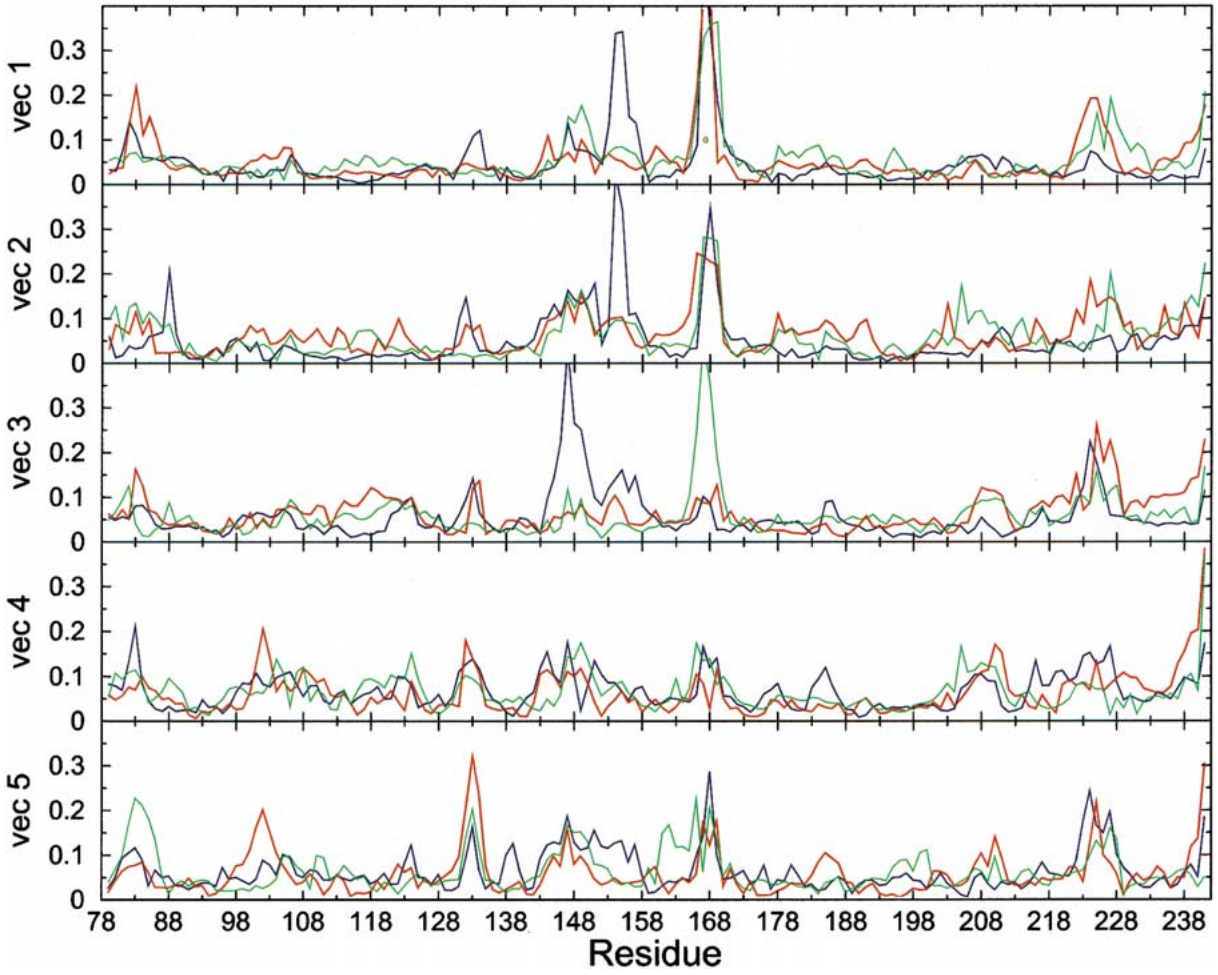

Figure 6. Components of the first five eigenvectors for the uncomplexed MMP-8 (blue line), S-side (green line) and S′-side (red line) PLTP-enzyme bound states.

H-bonds with the CO groups of Gln 166 (50% occurrence) and Ala 163 (80% occurrence), respectively; the latter H-bond is mediated by a water molecule. No conformational strain affects the PLTP binding in this region. The inhibitor Trp side-chain oscillates around the average χ^2 of 83° in agreement with the value ($\cong \pm 90°$) found in the crystal structures of peptides containing aromatic residues [30]. As expected, the bottleneck entrance of the primary specificity pocket S_1' is unaffected by the ligand. In fact, the distance between the carbonyl oxygens of Ala 161 and Pro 217, the two residues at the upper and lower side, respectively of the S_1' entrance, maintains a fairly constant value of 0.80 nm during the simulation. This value agrees with those found in MMP-8 crystal complexes containing undistorted S_1' entrance [16, 17, 31–35].

Enzyme-ligand interactions at the S′ side

In the MD simulation of PLTP interacting with the S′ region, the distance between the carbonyl oxygens of Ala 161 and Pro 217 increases to the average of 0.90 nm, a widening observed in the crystal of MMP-8 complexed with a sulfonamide inhibitor [12]. Inside the S_1' pocket, the Trp side-chain χ^2 oscillates around the average of 0°. This strained conformation, never found in crystal structures of peptides containing aromatic residues [30] occurs in the S_1' pocket of adamalysin complexed with FLTP [10] and with its carboxylate analogue [36] as well as in that of atrolysin complexed with pyroGlu-Asn- Trp [37]. The two H-bonds favouring the PLTP binding are engaged by the inhibitor Leu NH and CO groups with the

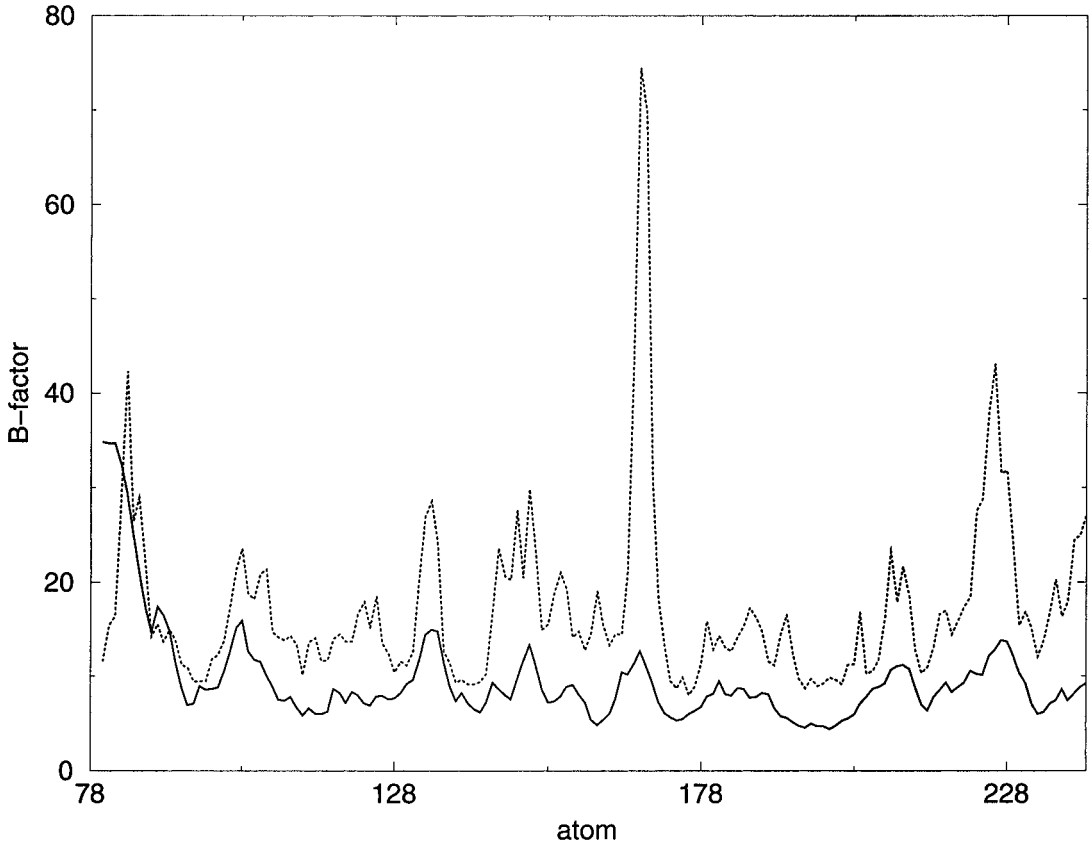

Figure 7. B factors of the C^{α} atoms determined from diffraction data collected at 100 K for the crystal complex MMP-8 :PLTP (full line) and simulated at 300 K for the same complex (dotted line) in aqueous solution.

Glu158 CO (59% occurrence) and Leu 160 NH groups (51% occurrence), respectively.

The distance between the catalytic zinc ion and the inhibitor phosphonate oxygen shows an average of 0.80 nm. This value, significantly larger than that obtained for PLTP interacting with the S-side (0.38 nm), indicates lack of coordination bond.

The S'_3 subsite is externally limited by the Tyr side-chain of the *cis* peptide bond Asn 188–Tyr 189. This rare non-Pro *cis* peptide bond is stabilized by the C-H$\cdots\pi$ interaction involving the π-cloud of Tyr 189 and the Asn 188C^{β}H atom [38, 39]. This interaction was monitored in the three simulations performed on the uncomplexed enzyme, S -and S′-side PLTP-enzyme bound states and the time course is shown in Figure 8. The first two systems (blue and green lines, respectively) show the same average of 0.38 nm, whereas in the last case this distance decreases to 0.25 nm (red line). This short unfavourable contact is caused by the accommodation of the inhibitor Pro ring in the S'_3 subsite, there pushing the Tyr 189 side-chain against the Asn 188C^{β}H atom. Therefore the beneficial occupation of the primary specificity pocket S'_1 by the inhibitor Trp side-chain and favourable enzyme-ligand H-bonds are contrasted by lack of catalytic zinc chelation, steric hindrance at the S'_3 subsite and strained conformations.

Inhibitor fluctuation

In order to account for the effect of enzyme-ligand interaction on PLTP fluctuation, we have reported in Figure 9 the rmsf of the free inhibitor in aqueous solution (full line) together with that of PLTP bound in the S- (dashed line) and S′-side (dotted line) of the active site. Each fluctuation is fitted to the initial minimized structure. As expected, the interaction with the enzyme drastically lowers the fluctuation of the inhibitor. However, when PLTP binds in the S′-side, the fluctuation of Trp side-chain, that is completely buried into the deep S'_1 pocket, appears almost entirely suppressed. In contrast, when PLTP binds in the S-side,

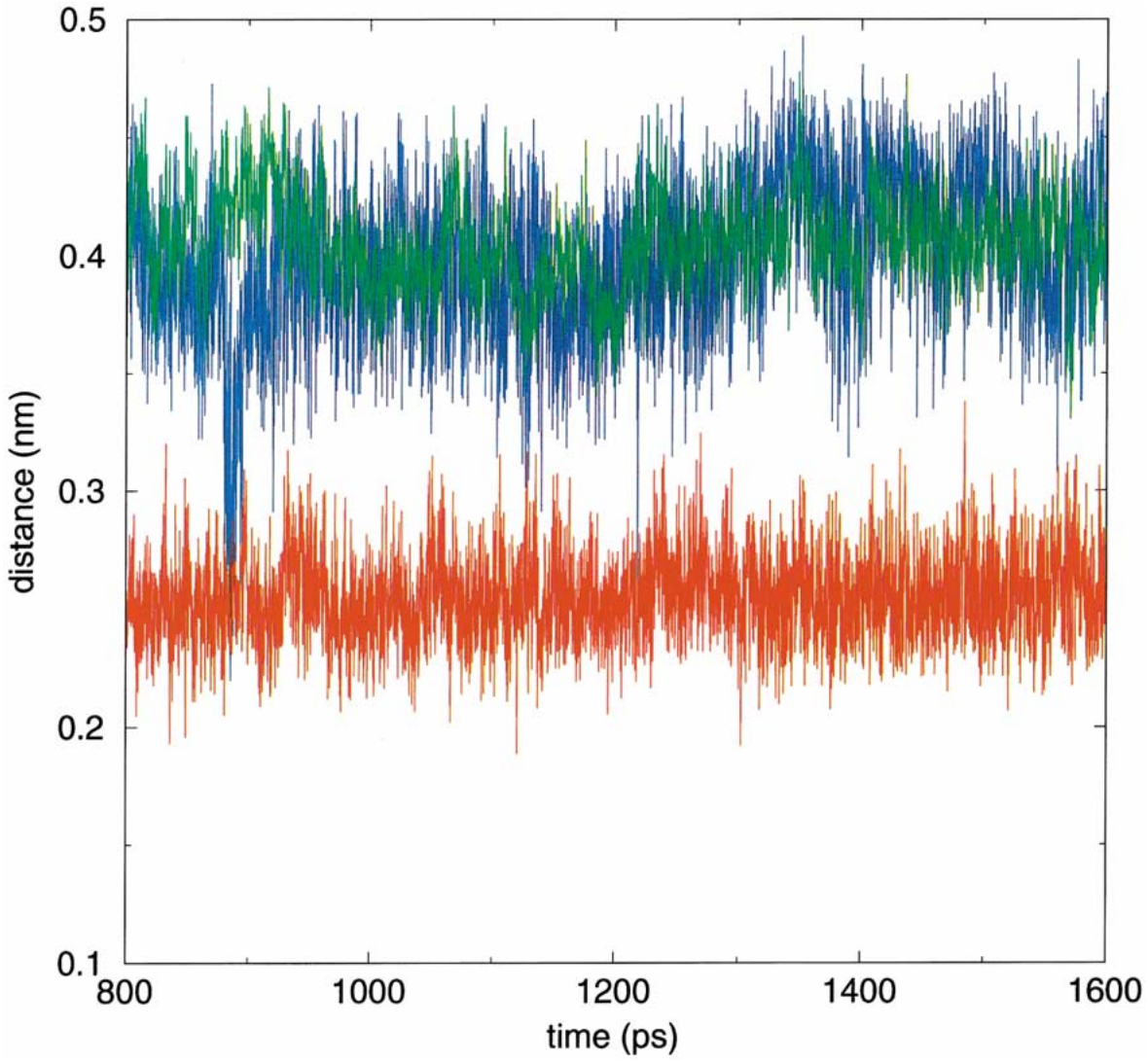

Figure 8. Time course of the distance between the Asn 188$C^{\beta}H$ atom and the center of the Tyr 189 aromatic ring in the three simulations performed on the uncomplexed enzyme (blue line), S- (green line) and S′-side (red line) PLTP-enzyme bound states.

the fluctuation of Trp side-chain appears similar to that of the free ligand. This MD result is in accordance with experimental data, since the Fourier map of the crystal complex MMP-8:PLTP [12] shows a scarcely defined electron density of Trp side-chain in the S-side. This is probably due to the shallow concavity of the S_1 subsite that is largely exposed to the solvent.

The fluctuation of the inhibitor Pro ring bound in the S_3 subsite (dashed line) was much higher than expected. Considering that the pyrrolidine ring is involved in a cation-π interaction with the Phe 164 π-cloud, its increased fluctuation could probably due to inadequate treatment of the cation-π interaction by the force field. In fact, the adopted force field includes the electrostatic term only, neglecting polarization and charge transfer terms which are significant components describing cation-π interaction [40].

Conclusions

The MD simulation performed on the uncomplexed catalytic domain of MMP-8 shows that it reaches a stable structure in aqueous solution, slightly differing from that found in the crystal complex MMP-8:PLTP [12]. Only the loops 144–160 and 164–173 show pro-

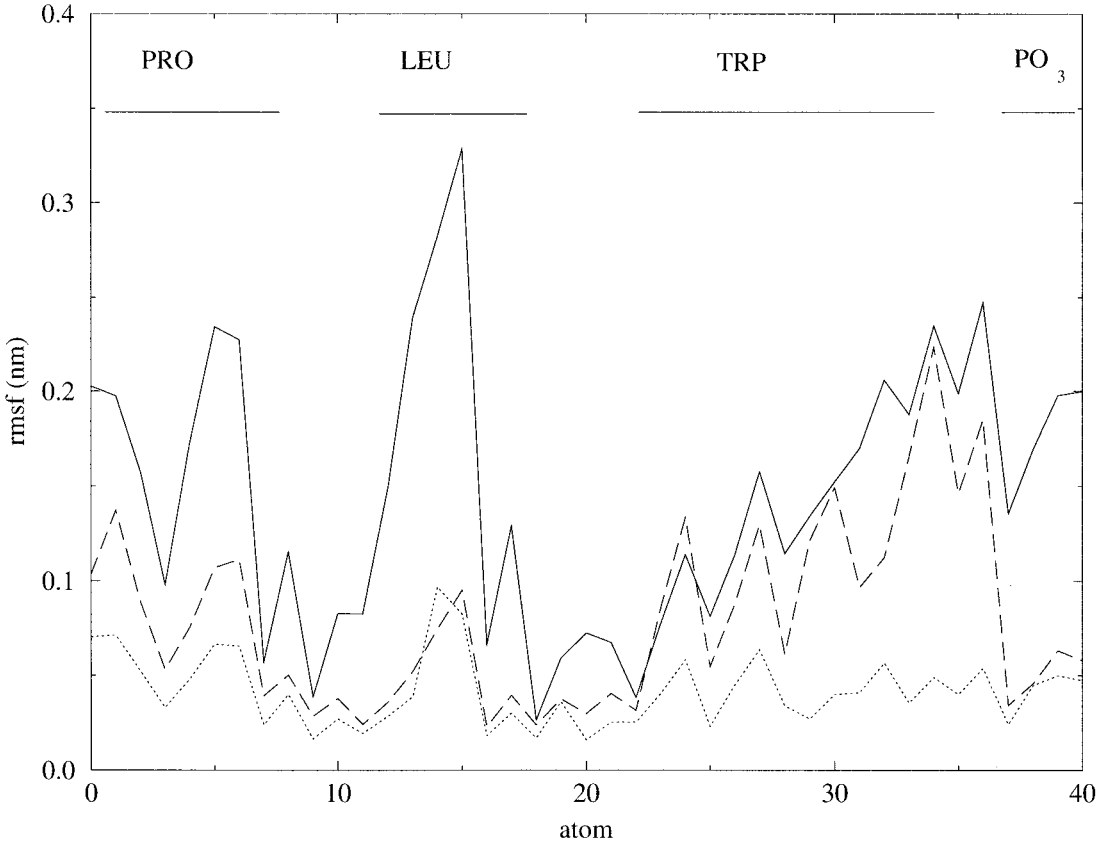

Figure 9. Root-mean square fluctuation (rmsf) of PLTP free in aqueous solution (full line), bound to the S′-side (dotted line) and S-side (dashed line) of MMP-8 active site. The atomic numbering is that shown in Figure 2. Side-chains and phosphonate group are indicated on top of the figure by horizontal lines.

nounced fluctuation in these conditions. The close resemblance between the crystal structure of MMP-8 and that simulated in aqueous solution, even in the absence of the inhibitor, renders the X-ray structure of this enzyme, and possibly other MMPs, particularly suitable for molecular modelling studies of new inhibitors.

The simulated interactions of PLTP with the S- and S′-side of the active site, cause a similar increase in the enzyme overall fluctuation. In both cases the main contribution to the overall fluctuation is supplied by the loop 164–173. A detailed analysis of the fluctuation of this loop reveals that it is spread over more degrees of freedom when PLTP interacts with the S-side. This dynamical aspect is in accordance with the complex formation at the S-side.

Catalytic zinc chelation, a cation-π interaction at the S_3 subsite and H-bonds together with unstrained binding conformations assist the PLTP ligation in the S-side. The unfavourable conditions encountered in the S′-side can be summarized as follows: (i) loss of the zinc-phosphonate oxygen chelation; (ii) conformational strains to widen the S'_1 pocket entrance and to promote the unusual conformation ($\chi^2 \approx 0°$) of the inhibitor Trp side-chain; (iii) steric hindrance at the S'_3 subsite caused by the accommodation of the inhibitor Pro ring.

The present study shows that tripeptide inhibitors bearing the Trp or phosphono-Trp as C-terminal residue, and capable of binding in the S′ subsites of reprolysins, are unsuitable for binding in the corresponding S′ subsites of MMP-8. The main factor affecting the binding mode of this type of inhibitors seems to be the architecture of both S_3 and S'_3 subsites. In fact, while the S_3 subsite stabilizes the insertion of the inhibitor Pro ring by an additional cation-π interaction, the S'_3 subsite disfavours its accommodation. The S_3 and S'_3 subsites of MMP-8 appear to play a role more important than that of the primary specificity

pocket S_1' in determining the mode of binding of the inhibitor.

Acknowledgements

This study was supported from MURST, CNR by the Targeted Program 'Biotecnologie', and EC by the TMR project 'Structure and Dynamics of Intermediate States in Protein Folding'.

References

1. Jiang, W. and Bond, J.S., FEBS Lett., 312 (1992) 110.
2. Bode, W., Gomis-Rüth, F.-X. and Stocker, W., FEBS Lett., 331 (1993) 134.
3. Stocker, W. and Bode, W., Curr. Opin. Struct. Biol., 5 (1995) 383.
4. Stöcker, W., Grams, F., Baumann, U., Reinemer, P., Gomis-Rüth, F.-X., McKay, D.B. and Bode, W., Protein Sci., 4 (1995) 823.
5. Robeva, A., Politi, V., Shannon, J.D., Bjarnason, J.B. and Fox, J.W., Biomed. Biochim. Acta, 50 (1991) 769.
6. Politi, V., Gavuzzo, E., D'Alessio, S., Sella, A., Piazza, C., Giordano, C., Gorini, B., Panini, G., Paglialunga P., M., Cirilli, M., Pochetti, G. and Mazza, F., PCT Int. Appl. WO 99/03878.
7. D'Alessio, S., Gallina, C., Gavuzzo, E., Giordano, C., Gorini, B., Mazza, F., Paglialunga P., M., Panini, G., Pochetti, G. and Sella, A., Bioorg. Med. Chem., 7 (1999) 389.
8. Gomis-Rüth, F.-X., Kress, L.F. and Bode, W., EMBO J., 12 (1993) 4151.
9. Gomis-Rüth, F.-X., Kress, L.F., Kellermann, J., Mayr, I., Lee, X., Huber, R. and Bode, W., J. Mol. Biol., 239 (1994) 513.
10. Cirilli, M., Gallina, C., Gavuzzo, E., Giordano, C., Gomis-Rüth, F.-X., Gorini, B., Kress, L.F., Mazza, F., Paglialunga P., M., Pochetti, G. and Politi, V., FEBS Lett., 418 (1997) 319.
11. Gallina, C., Gavuzzo, E., Giordano, C., Gorini, B., Mazza, F., Paglialunga P.M., Panini, G., Pochetti, G., Ann. N.Y. Acad. Sci., 878 (1999) 700.
12. Gavuzzo, E., Pochetti, G., Mazza, F., Gallina, C., Gorini, B., D' Alessio, S., Pieper, M., Tschesche, H. and Tucker, P.A., J. Med. Chem. 43 (2000) 3377.
13. Netzel-Arnett, S., Fields, G. B., Birkedal-Hansen, H. and van Wart, H.E., J. Biol. Chem., 266 (1991) 6747.
14. Niedzwiecki, L., Teahan, J., Harrison, R.K. and Stein, R.L., Biochemistry, 31 (1992) 12618.
15. Netzel-Arnett, S., Sang, Q.-X., Moore, W.G.I., Navre, M., Birkedal-Hansen, H. and van Wart, H.E., Biochemistry, 32 (1992) 6427.
16. Grams, F., Reinemer, P., Powers, J.C., Kleine, T., Pieper, M., Tschesche, H., Huber, R. and Bode, W., Eur. J. Biochem., 228 (1995) 830.
17. Grams, F., Crimmin, M., Hinnes, L., Huxley, P., Pieper, M., Tschesche, H. and Bode, W., Biochemistry, 34 (1995) 14012.
18. van Gusteren, W.F. and Berendsen, H.J.C., Gromos Manual. BIOMOS, Biomolecular Software, Laboratory of Physical Chemistry, University of Groeningen, The Netherlands, 1987.
19. Hoops, S.C., Anderson, K.W. and Merz, K.M., J. Am. Chem. Soc., 113 (1991) 8262.
20. Breneman, C.M. and Wilberg, K.B., J. Comput. Chem., 11 (1990) 361.
21. Schmidt, M.W., Baldridge, K.K., Boatz, J.A., Elbert, S.T., Gordon, M. S., Jensen, J.H., Koseki, S., Matsunaga, N., Nguyen, K.A, Su, S., Windus, T.L., Dupuis, M. and Montgomery, J.A., J. Comput. Chem., 14 (1993) 1347.
22. Berendsen, H.J.C., Postma, J.P.M., van Gusteren, W.F. and Hermans, J., In Pullman, B. (Ed.), Intermolecular Forces, D. Reidel Publ. Co., Dordrecht, 1981, pp. 331–342.
23. Allen, M.P. and Tildesley, D.S. (Eds.), Computer Simulation of Liquids, Oxford University Press, Oxford, 1989, pp. 212–239.
24. Ryckaert, J.P., Ciccotti, G. and Berendsen, H.J.C., J. Comp. Phys., 23 (1977) 327.
25. Amadei, A., Chillemi, G., Ceruso, M.A., Grottesi, A. and Di Nola, A., J. Chem. Phys., 112 (2000) 9.
26. Amadei, A., Linssen, A.B.M. and Berendsen, H.J.C., Proteins: Struct. Funct. Gen., 17 (1993) 412.
27. van der Spoel, D., van Drunen, R. and Berendsen, H.J.C., GROningen machine for chemical simulations. Department of Biophysical Chemistry, BIOSON Research Institute, Nijenborg 4 NL-9717 AG Groningen, 1994.
28. Kabsch, W. and Sander, C., Biopolymers, 22 (1983) 2576.
29. Roccatano, D., Mark, A.E. and Hayward, S., J. Mol. Biol, 310 (2001) 1039.
30. Ashida, T., Tsunogae, Y., Tanaka, I. and Yamane, T., Acta Crystallogr., B43 (1997) 212.
31. Bode, W., Reinemer, P., Huber, R., Kleine, T., Schnierer, S. and Tschesche, H., EMBO J., 13 (1994) 1263.
32. Reinemer, P., Grams, F., Huber, R., Kleine, T., Schnierer, S., Pieper, M., Tschesche, H. and Bode, W., FEBS Lett., 338 (1994) 227.
33. Starns, T., Spurlino, J.C., Smith, D.L., Wahl, R.C., Ho, T.F., Qoronfleh, M.W., Banks, T.-M. and Rubinn, B., Nat. Struct. Biol., 1 (1994) 119.
34. Betz, M., Huxley, P., Davies, S.J., Mushtaq, Y., Pieper, M., Tschesche, H., Bode, W. and Gomis-Rüth, F.-X., Eur. J. Biochem., 247 (1997) 356.
35. Brandstetter, H., Engh, R.A., Graf Von Roedern, E., Moroder, L., Huber, R., Bode, W. and Grams, F., Protein Sci., 7 (1998) 1303.
36. Gomis-Rüth, F.-X., Meyer, E.F., Kress, L.F. and Politi, V., Protein Sci., 7 (1998) 283.
37. Zhang, D., Botos, I., Gomis-Rüth, F.-X., Doll, R., Blood, C., Njoroge, F.G., Fox, J.W., Bode, W. and Meyer, E.F., Proc. Natl. Acad. Sci. USA, 91 (1994) 8447.
38. Weiss, M.S. and Hilgenfeld, R., Biopolymers, 50 (1999) 536.
39. Jabs, A., Weiss, M.S. and Hilgenfeld, R., J. Mol. Biol., 286 (1999) 291.
40. Aschi, M., Mazza, F. and Di Nola, A., J. Mol. Struct. (THEOCHEM) 587 (2002) 177.